SUPPORTING INFORMATION

SENSITIVITY ANALYSIS

Sensitivity analysis is performed to identify the effects of the different input parameters on the model results, and all of the input parameters are set accordingly (Table S1).

Table S1. Tested range, chosen values and results of the sensitivity analysis of input parameters.

Input Parameters	Tested Range	Chosen Values	Sensitivity Analysis
Specific density (kg/m^3)	2500 to 2880	2690	No significant influence
Dry bed density (kg/m^3)	1800 to 2600	2120	No significant influence
Settling velocity (mm/s)	0.15 to 0.36	0.15	Higher settling velocity can lead to greater sedimentation rate, but weakly impacts the bed shear stress and stability of water level.
Roughness length, z_0 (m)	5×10^{-3} to 2×10^{-6}	5×10^{-3}	Higher roughness length can lead to higher bed shear stress but less stable water level.
Horizontal eddy viscosity (m^2/s)	1 to 10	1	A lower horizontal eddy viscosity makes the water level more stable and leads to a more fluctuating bed shear stress.
Horizontal eddy diffusivity (m^2/s)	1 to 10	1	Horizontal eddy diffusivity hardly influences the bed shear stress and water level, but creates less warnings in the simulation when it is low.
Critical bed shear stress for erosion (N/m^2)	0.02 to 0.15	0.06	Lower critical bed shear stress for erosion can increase the erosion rate.

Table S1. (Continued).

Input Parameters	Tested Range	Chosen Values	Sensitivity Analysis
Critical bed shear stress for sedimentation (N/m^2)	0.025 to 0.05	0.04	Higher critical bed shear stress for sedimentation can increase sedimentation rate.
Erosion parameter (kg/m^2s)	0.0001 to 1	0.0004	Higher erosion parameter increases the erosion rate when bed shear stress is larger than critical value of erosion.
Morphological time-scale factor	1 to 10000	3000	Higher morphological time scale factor magnifies the feedback of seabed (morphological change) under the erosional and depositional processes induced by ocean currents.
Input current velocity (m/s)	0.12 to 0.18	0.156, 0.158 and 0.160	The value of current velocity determines speed of the near-seafloor currents and bed shear stress.

Sediment density: The input parameters of sediment density include dry bed density and specific density. Dry bed density indicates the density of sediments above the fixed seafloor, and specific density corresponds to sediment fractions in the fluid mixture for sediment transportation (Deltares, 2014). The dry bed density is usually defined as "wet bulk density" in many related references. It is equal to sediment mass per unit volume in the raw state and depends on particle density, porosity volume, and pore water composition (Hou et al., 2015). Moreover, the measured sediment bulk density (from wireline logs) in the northern South China Sea is between 1800 and 2100 kg/m^3 (Wang et al., 2011). According to the core data in the western South China Sea and close to the study area (Bassinot and Chen, 2002), the wet bulk density (at depths of 2 to 10 m below the seafloor) is in the range of 1800 and 2600 kg/m^3. According to the test results of different dry bed densities (ranging from 1800 to 2600 kg/m^3), the change of dry bed density can hardly influence the simulation results. Therefore, we set the average value of 2120 kg/m^3 as the chosen value of dry bed density for this study.

Moreover, the specific density of sediment fractions is indicated by the sediment grain density, which is between 2640 and 2810 kg/m^3 for fine-grained (<62 μm) sediment particles (Dagg et al., 1996). From ODP 184, the sediment grain density for the South China Sea is in the range between 2500 and 2880 kg/m^3 (Huang et al., 2006). According to the testing simulations, the values of specific density in the range between 2500 and 2880 kg/m^3 can hardly influence the simulation results. Therefore, the average value of 2690 kg/m^3 is chosen as the specific density for the simulation.

Settling velocity: In this study, the settling velocity in fresh water and salinity concentration have been set equal to disregard the influence of flocculation on the simulation, considering the low concertation of bottom currents. The settling velocity of a spherical sediment grain in a fluid (w_s, from Stokes' law; e.g., Shepard 1963) is defined as:

$$w_s = \frac{(\rho_s - \rho_f) g d^2}{18\mu_f} \tag{1}$$

Where, ρ_s is sediment grain density (~2690 kg/m^3 for specific density); ρ_f is fluid density (~1026 kg/m^3 for seawater at 5°C); g is acceleration of gravity (9.81 m/s^2); d is sediment grain size (5 µm); μ_f is dynamic fluid viscosity (~0.0015 kg m^{-1} s^{-1} for seawater at 5°C). Therefore, the calculated settling velocity is ~0.15 mm/s.

Moreover, the observed settling velocity of fine-grained sediments (mean grain size between 7.0 and 9.6 µm) in a coastal salt marsh varies from 0.17 to 0.32 mm/s, with a mean value of 0.26 mm/s (Wang et al., 2010). Through 3-D numerical simulations, Yu et al. (2014) investigated the sedimentation of silt with mean grain size of 20 µm in saltwater, and obtained a settling velocity of 0.36 mm/s. In order to assess the influence of settling velocity, we have tested settling velocities ranging from 0.15 to 0.36 mm/s. Test results indicate that the lowest settling velocity has a weak influence on bed shear stress and stability of the simulation. Therefore, the settling velocity is set as 0.15 mm/s in this study, and it is combined with a constant sediment input of 0.02 kg/m^3 according to the previous study of Chen et al. (2016).

Roughness length: Based on the wide range of studies at the Plymouth Marine Laboratory (PML) about the sediment types concluded by Pope et al. (2006), the roughness length (z_0) of a seabed with cohesive sediment has values between 1 and 180 µm. Moreover, the roughness length can be increased by a factor of 2 to 30 due to the presence of biogenic structures on the seafloor (Peine et al., 2009).

Therefore, the possible range of roughness length (z_0) tested for the simulation is between 2×10^{-6} and 5×10^{-3} m. According to the tests of roughness length, the bed shear stress increases with higher roughness lengths. In order to effectively investigate the bottom current erosion on the seafloor, the roughness length of 0.005 m was chosen for this study. The chosen value of roughness length is close to the roughness length of abyssal seafloor (ca. 0.003 m) given by Connolly et al. (2020), and the roughness length of 0.005 m also has been measured on the seafloor with sparse benthic life (Schönke et al., 2019).

Eddy viscosity and diffusivity: Based on the manual of Delft3D-FLOW (Deltares, 2014), the values for both the horizontal eddy viscosity and diffusivity are determined by the grid size used in the simulation. For detailed models with grid sizes typically tens of meters or less, the values for the eddy viscosity and the eddy diffusivity are typically in the range of 1 to 10 m^2/s.

Corresponding to the grid size of 2 meters for this study, the value of horizontal eddy viscosity and diffusivity have been tested in the range of 1 to 10 m^2/s. When horizontal eddy viscosity and diffusivity are both set at 1 m^2/s, the simulation results show a steady water level and fluctuations in bed shear stress above the pockmark.

Critical bed shear stress: The critical bed shear stresses for erosion and sedimentation control the erosional and sedimentary processes. Sedimentation only occurs when bed shear stress is lower than the critical stress of sedimentation, and erosion only happens when bed shear stress is larger than the critical stress of erosion (Deltares, 2014).

The critical bed shear stress for erosion and sedimentation is controlled by many factors, such as grain size, sediment composition, depositional history, seabed roughness, viscosity of currents and even biological activity (Durrieu de Madron et al., 2017). Previous studies show that the critical bed shear stress of erosion for cohesive sediments ranges from 0.02 to 0.15 N/m^2, and the mean value of critical bed shear stress of erosion for cohesive sediment is ~0.06 N/m^2 (Table S2). According to the previous studies, the critical bed shear stress for sedimentation of cohesive sediments ranges from 0.025 to 0.05 N/m^2 (Table S3), with an average value of ~0.04 N/m^2.

In order to simulate the erosion and sedimentation in the seabed dominated by cohesive sediments objectively, the critical bed shear stresses for erosion and sedimentation are set as 0.06 and 0.04 N/m^2, respectively, which are average value of previous studies (Tables S2 and S3).

Table S2. Critical bed shear stress for erosion for fine-grained sediment obtained in previous studies.

Previous studies	Grain size (μm)	Critical bed shear stress for erosion (N/m^2)
Krone (1962)	Cohesive sediments	0.06 to 0.078
Houwing and Rijn (1995)	Cohesive sediments	0.06 to 0.12
Otsubo and Muraoka (1988)	10 to 40	0.035 to 0.15
Lau and Droppo (2000)	Cohesive sediments	0.035
Schaaff et al. (2002)	4 to 20	0.022 to 0.038
El Ganaoui et al. (2004)	15 to 55	0.025 to 0.04
Araújo et al. (2008)	32 to 41	0.043 to 0.058
Chen et al. (2016)	60 (D50)	0.06
Durrieu de Madron et al. (2017)	10 (D50)	0.07 to 0.11

Table S3. Critical bed shear stress for sedimentation for fine-grained sediment obtained in previous studies.

Previous studies	Grain size (μm)	Critical bed shear stress for sedimentation (N/m^2)
Krone (1962)	Cohesive sediments	0.04
Adamsson et al. (2003)	47 (D50)	0.03 to 0.05
Chan et al. (2006)	2.8 (D50)	0.0442
Maa et al. (2008)	4 (D50)	0.04
Shi et al. (2012)	15 to 23 (D50)	0.05
Hung et al. (2014)	35 (D50)	0.025

Erosion parameter: In Delft3D-FLOW, the erosion parameter is a user-defined value that affects the erosion rate of sediment (Deltares, 2014):

$$E = M(\frac{\tau_b}{\tau_e} - 1), \text{ when } \tau_b > \tau_e \quad (2)$$

Where, E is erosion flux (kg/m^{2}s), M is erosion parameter (kg/m^{2}s), τ_b is bed shear stress and τ_e is critical bed shear stress for erosion. Therefore, an appropriate erosion parameter can decrease simulation time and increase the erosion rate. Through the testing simulations with the erosion parameters ranging from 0.0001 to 1 kg/m^{2}s, the most appropriate erosion parameter is set as 0.0004 kg/m^{2}s in this study.

Morphological time scale factor: In many previous modelling studies, morphological time-scale factor has been commonly used for accelerating the simulation of long-term morphological evolution, while avoiding the disturbance on modeling results (Van Der Wegen and Roelvink, 2008; Zhang et al., 2010). In Delft3D, the implementation of the morphological time-scale factor is achieved by multiplying the erosion and deposition fluxes from the bed to the flow by a constant factor (Roelvink, 2006; Briere et al., 2011; Deltares, 2014; Morgan et al., 2020). Therefore, the value of morphological time scale factor determines the rate of morphological change under the erosion and deposition of modeled bottom currents. In this study, through the testing simulation, the morphological time scale factor is set as 3000. With the setting of morphological time scale factor and erosion parameters, the modelling for long-term morphological evolution lasting tens of years can be shortened into 72 hours.

Input current velocity: According to the Acoustic Doppler Current Profiler (ADCP) data collected by Yang et al. (2019), the annual average velocity of ocean current (in the water depth between 750 and 1000 m) in the NW South China Sea (2009-2013) ranges between 0.12 and 0.18 m/s (Fig. 3). Therefore, in order to reveal the actual oceanographic settings, the input velocities of currents ranging from 0.12 to 0.18 m/s were tested (Table S4). The test results reveal that bottom layer velocity and bed shear stress are positively related to the input current velocity. Through the test of current velocity, three input current velocities were chosen for the simulations to reveal three different morphodynamical situations for the bottom current erosion on pockmarks, which are 0.120, 0.158 and 0.170 m/s.

Table S4. Bottom layer velocity and bed shear stress obtained for different initial current velocities.

Current velocity (m/s)	Bottom layer velocity (m/s)		Bed shear stress (N/m^2)	
	Max.	Min.	Max.	Min.
0.12	0.066	0.056	0.038	0.026
0.13	0.072	0.062	0.045	0.031
0.14	0.078	0.065	0.052	0.036
0.15	0.084	0.070	0.060	0.041
0.16	0.090	0.075	0.069	0.047
0.17	0.095	0.079	0.078	0.053
0.18	0.100	0.084	0.090	0.060

Table S5. Geometrical parameters of 25 observed pockmarks.

Pockmark	Water Depth (m)	Diameter (m)	Depth (m)	Diameter/Depth Ratio
1	850	850	80	10.63
	810	1000	120	8.33
2	910	700	65	10.77
	890	670	80	8.38
3	860	800	85	9.41
	860	1000	90	11.11
4	850	850	80	10.63
	810	1000	120	8.33
5	935	720	77	9.35
	925	770	90	8.56
6	975	1125	55	20.45
	950	820	77	10.65
7	780	1200	135	8.89
	795	1100	120	9.17
8	776	830	64	12.97
	787	700	52	13.46
9	900	680	50	13.60
	900	640	50	12.80
10	850	1100	102	10.78
	832	1200	121	9.92
11	825	880	88	10.00
	817	1260	95	13.26
12	860	1200	100	12.00
	850	1000	110	9.09
13	903	810	75	10.80
	908	800	70	11.43
14	894	856	92	9.30
	905	1110	84	13.21
15	832	905	110	8.23
	850	1080	93	11.61
16	768	894	46	19.43
	770	900	47	19.15
17	777	940	79	11.90
	780	1150	75	15.33
18	878	1090	80	13.63
	892	695	67	10.37
19	872	740	71	10.42
	877	780	65	12.00

Table S5. (Continued)

Pockmark	Water Depth (m)	Diameter (m)	Depth (m)	Diameter/Depth Ratio
20	800	989	71	13.93
	810	963	62	15.53
21	783	937	40	23.43
	784	1220	40	30.50
22	1016	838	48	17.46
	1016	1065	47	22.66
23	827	890	66	13.48
	838	910	53	17.17
24	863	880	62	14.19
	860	853	70	12.19
25	925	500	45	11.11
	910	666	60	11.10
Mean value	858.7	911.12	76.48	12.84

ADDITIONAL FIGURE

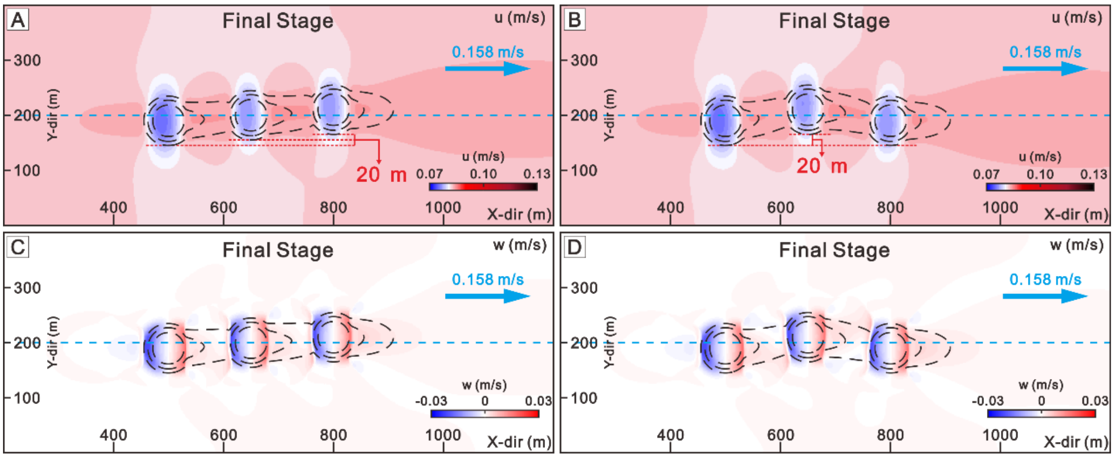

Figure S1. Streamwise horizontal velocity (u) and vertical velocity (w) at the final stages of the morphological evolution of pockmark trains, which are oblique to current direction (A and C) and not in a straight line (B and D), with a lateral deviation of 20 m. The blue dashed lines indicate the axis of domain, and the coalesced pockmarks are marked by the dark dashed contours. The blue arrow indicates a leftward direction (parallel to the domains axis) of input currents. Consequently, the channel inception induced by bottom current erosion also can occur, even though the pockmarks are not aligned in a straight line parallel to the current direction.

REFERENCES CITED

Adamsson, Å., Stovin, V. & Bergdahl, L. (2003) Bed shear stress boundary condition for storage tank sedimentation. *Journal of Environmental Engineering*, v. 129, no. 7, p. 651-658. Avaliable from: https://doi.org/10.1061/(ASCE)0733-9372(2003)129:7(651).

Araújo, M.A.V.C., Teixeira, J.C.F. & Teixeira, S.F.C.F. (2008) Application of laser anemometry for measuring critical bed shear stress of sediment core samples. *Continental Shelf Research*, v. 28, no. 20, p. 2718-2724. Avaliable from: https://doi.org/10.1016/j.csr.2008.09.011.

Bassinot, F.C. & Chen, M-T. (2002) Physical properties of sediment, core MD01-2395. *PANGAEA*, Avaliable from: https://doi.org/10.1594/PANGAEA.68577.

Betzler, C., Lindhorst, S., Hübscher, C., Lüdmann, T., Fürstenau, J. & Reijmer, J. (2011) Giant pockmarks in a carbonate platform (Maldives, Indian Ocean). *Marine Geology*, 289(1-4), p. 1-16. Avaliable from: https://doi.org/10.1016/j.margeo.2011.09.004.

Briere, C., Giardino, A. & van der Werf, J. (2011) Morphological modeling of bar dynamics with DELFT3d: the quest for optimal free parameter settings using an automatic calibration technique. *Coastal Engineering Proceedings: sediment*, 1(32), 1-12. Avaliable from: https://doi.org/10.9753/icce.v32.sediment.60.

Chan, W.Y., Wai, O.W.H. & Li, Y.S. (2006) Critical Shear Stress for Deposition of Cohesive Sediments in Mai Po. *Journal of Hydrodynamics*, Ser. B, v. 18, no. 3, p. 300-305. Avaliable from: https://doi.org/10.1016/S1001-6058(06)60070-X.

Chen, H., Xie, X., Zhang, W., Shu, Y., Wang, D., Vandorpe, T. & Van Rooij, D. (2016) Deep-water sedimentary systems and their relationship with bottom currents at the intersection of Xisha Trough and Northwest Sub-Basin, South China Sea. *Marine Geology*, 378, 101-113. Avaliable from: https://doi.org/10.1016/j.margeo.2015.11.002.

Connolly, T. P., McGill, P. R., Henthorn, R. G., Burrier, D. A. & Michaud, C. (2020) Near-bottom currents at Station M in the abyssal Northeast Pacific. *Deep Sea Research Part II: Topical Studies in Oceanography*, 173, 104743. Avaliable from: https://doi.org/10.1016/j.dsr2.2020.104743.

Dagg, M.J., Green, E., McKee, B. & Ortner, P. (1996) Biological removal of fine-grained lithogenic particles from a large river plume. *Journal of Marine Research*, v. 54, no. 1, p. 149-160. Avaliable from: https://doi.org/10.1357/0022240963213466.

Deltares. (2014) User manual Delft3D-FLOW. Delft, The Netherlands: Deltares, p. 329-331. Avaliable from: https://content.oss.deltares.nl/delft3d/manuals/Delft3D-FLOW_User_Manual.pdf.

Durrieu De MaSon, X., Ramondenc, S., Berline, L., Houpert, L., Bosse, A., Martini, S., Guidi, L., Conan, P., Curtil, C., Delsaut, N., Kunesch, S., Ghiglione, J. F., Marsaleix, P., Pujo-Pay, M., Séverin, T., Testor, P., Tamburini. C. & ANTARES collaboration. (2017) Deep sediment resuspension and thick nepheloid layer generation by open-ocean convection. *Journal of Geophysical Research: Oceans*, 122(3), 2291-2318. Avaliable from: https://doi.org/10.1002/2016JC012062.

El Ganaoui, O., Schaaff, E., Boyer, P., Amielh, M., Anselmet, F. & Grenz, C. (2004) The deposition and erosion of cohesive sediments determined by a multi-class model. *Estuarine, Coastal and Shelf Science*, 60(3), 457-475. Avaliable from: https://doi.org/10.1016/j.ecss.2004.02.006.

Hou, Z., Guo, C., Wang, J., Chen, W., Fu, Y. & Li, T. (2015) Seafloor sediment study from South China Sea: Acoustic & physical property relationship. *Remote sensing*, 7(9), 11570-11585. Avaliable from: https://doi.org/10.3390/rs70911570.

Houwing, E-J. & Rijn, L.C.V. (1995) In-situ determination of the critical bed-shear stress for erosion of cohesive sediments. *Coastal Engineering Proceedings*, (24). Avaliable from: https://doi.org/10.1061/9780784400890.150.

Huang, W. & Wang, P. (2006) Sediment mass and distribution in the South China Sea since the Oligocene. *Science in China Series D: Earth Sciences*, 49(11), 1147-1155. Avaliable from: https://doi.org/10.1007/s11430-006-2019-4.

Hung, N.N., Delgado, J.M., Güntner, A., Merz, B., BárdosDRY, A. & Apel, H. (2014) Sedimentation in the floodplains of the Mekong Delta, Vietnam Part II: deposition and erosion. *HySological Processes*, v. 28, no. 7, p. 3145-3160. Avaliable from: https://doi.org/10.1002/hyp.9855.

Krone, R. (1962) Flume studies of the transport of sediment in estuarial processes: HySaulic Engineering Laboratory and Sanitary Engineering Research Laboratory, University of California, Berkeley, California.

Lau, Y.L. & Soppo, I.G. (2000) Influence of antecedent conditions on critical shear stress of bed sediments. *Water Research*, v. 34, no. 2, p. 663-667. Avaliable from: https://doi.org/10.1016/S0043-1354(99)00164-5.

Maa, J.P-Y., Kwon, J-I., Hwang, K-N. & Ha, H-K. (2008) Critical Bed-Shear Stress for Cohesive Sediment Deposition under Steady Flows. *Journal of HySaulic Engineering*, v. 134, no. 12, p. 1767-1771. Avaliable from: https://doi.org/10.1061/(ASCE)0733-9429(2008)134:12(1767).

Morgan, J. A., Kumar, N., Horner-Devine, A. R., Ahrendt, S., Istanbullouglu, E. & Bandaragoda, C. (2020) The use of a morphological acceleration factor in the simulation of large-scale fluvial morphodynamics. *Geomorphology*, 356, 107088. Avaliable from: https://doi.org/10.1016/j.geomorph.2020.107088.

Otsubo, K. & Muraoka, K. (1988) Critical shear stress of cohesive bottom sediments. *Journal of HySaulic Engineering,* v. 114, no. 10, p. 1241-1256. Avaliable from: https://doi.org/10.1061/(ASCE)0733-9429(1988)114:10(1241).

Peine, F., FrieSichs, M. & Graf, G. (2009) Potential influence of tubicolous worms on the bottom roughness length z0 in the south-western Baltic Sea. *Journal of Experimental Marine Biology and Ecology*, v. 374, no. 1, p. 1-11. Avaliable from: https://doi.org/10.1016/j.jembe.2009.03.016.

Pope, N.D., Widdows, J. & Brinsley, M.D. (2006) Estimation of bed shear stress using the turbulent kinetic energy approach—A comparison of annular flume and field data. *Continental Shelf Research*, v. 26, no. 8, p. 959-970. Avaliable from: https://doi.org/10.1016/j.csr.2006.02.010.

Roelvink, J. A. (2006) Coastal morphodynamic evolution techniques. *Coastal engineering*, 53(2-3), 277-287. Avaliable from: https://doi.org/10.1016/j.coastaleng.2005.10.015.

Schaaff, E., Grenz, C. & Pinazo, C. (2002) Erosion of particulate inorganic and organic matter in the Gulf of Lion. *Comptes Rendus Geoscience*, 334(15), p. 1071-1077. Avaliable from: https://doi.org/10.1016/S1631-0713(02)01853-9.

Schönke, M., Wiesenberg, L., Schulze, I., Wilken, D., Darr, A., Papenmeier, S. & Feldens, P. (2019) Impact of Sparse Benthic Life on Seafloor Roughness and High-Frequency Acoustic Scatter. *Geosciences*, 9(10), p. 454. Avaliable from: https://doi.org/10.3390/geosciences9100454.

Shepard, F.P., (1963) Submarine geology: New York, Harper and Row, p. 517. Avaliable from: https://library.wur.nl/link/link_router/index/20563597.

Shi, B.W., Yang, S.L., Wang, Y.P., Bouma, T.J. & Zhu, Q. (2012) Relating accretion and erosion at an exposed tidal wetland to the bottom shear stress of combined current–wave action. *Geomorphology*, v. 138, no. 1, p. 380-389. Avaliable from: https://doi.org/10.1016/j.geomorph.2011.10.004.

Van Der Wegen, M. & Roelvink, J.A. (2008) Long-term morphodynamic evolution of a tidal embayment using a two-dimensional, process-based model. *Journal of Geophysical Research*, 113(C3). Avaliable from: https://doi.org/10.1029/2006JC003983.

Wang, A., Ye, X. & Chen, J. (2010) Observations and analyses of floc size and floc settling velocity in coastal salt marsh of Luoyuan Bay, Fujian Province, China. *Acta Oceanologica Sinica*, v. 29, no. 3, p. 116-126. Avaliable from: https://doi.org/10.1007/s13131-010-0043-x.

Wang, X., Hutchinson, D.R., Wu, S., Yang, S. & Guo, Y. (2011) Elevated gas hySate saturation within silt and silty clay sediments in the Shenhu area, South China Sea. *Journal of Geophysical Research*, v. 116, no. B5. Avaliable from: https://doi.org/10.1029/2010JB007944.

Yang, Y., Xu, C., Li, S. & He, Y. (2019) Ship-mounted ADCP data for ocean currents in the South China Sea (2009 – 2012). *Science Data Bank*, (March 8, 2019). Avaliable from: http://www.doi.org/10.11922/sciencedb.740.

Yu, X., Hsu, T.-J. & Balachandar, S. (2014) Convective instability in sedimentation: 3-D numerical study. *Journal of Geophysical Research: Oceans*, v. 119, no. 11, p. 8141-8161. Avaliable from: https://doi.org/10.1002/2014JC010123.

Zhang, W., Harff, J., Schneider, R. & Wu, C. (2010) Development of a modelling methodology for simulation of long-term morphological evolution of the southern Baltic coast. *Ocean Dynamics*, 60(5), 1085-1114. Avaliable from: https://doi.org/10.1007/s10236-010-0311-5.